

CTF Surface Contamination and External Backgrounds

The preceding chapter included a thorough analysis of internal events in the CTF, those happening in the volume of scintillator. In this chapter we examine some characteristics of the surface and external contributions to events observed in the CTF. Recall that surface events are defined as those produced by radioactive materials embedded in the nylon vessel film, while external events are produced by radioactive decays outside the vessel.

Given that the range of an α particle in water or scintillator is negligible, while that of a β particle is on the order of millimeters, these particles will not be detected within the scintillator fluid if they originate outside the nylon vessel. They therefore make no contribution to the observed external activity, only to the surface activity. The observed rate of β emissions from the nylon film will be roughly half the true surface event rate: a β particle emitted from the nylon film has slightly less than a 50% chance of being directed inward into the scintillator, where it can be detected, instead of outward into the water buffer or sideways into the nylon where it is invisible. An α particle, with a range on the order of $100\ \mu\text{m}$, is only likely to be detected if it originates from the thin skin of nylon film closest to the scintillator volume, as well as being directed inward. In addition, an α produced within the nylon film will lose energy before making its way into the scintillator (even assuming

it can do so), leading to a low-energy tail of events in the α energy spectrum. In this chapter, we therefore presume that observed coincidences at the surface originate mostly from atoms adhering to the inner surface of the nylon vessel, not from those embedded within the vessel's nylon film.

The only radiation produced external to the nylon vessel that has a chance to be detected, and therefore the only contribution to the set of external events, is in the form of γ rays. These may travel many centimeters from their origins, permitting them to enter the volume of scintillator. Once inside the scintillator, a γ -ray photon will often scatter several times, producing more scintillation light each time, before being completely absorbed. A γ ray detected within the scintillator may also have first been scattered several times in the external water buffer. As a result, events that might be expected to produce a monoenergetic γ line are instead smeared out across lower energies. This characteristic makes an external γ -ray background intractable to analytic methods, and one must resort either to crude approximations or to Monte Carlo simulations in order to understand the observed energy spectrum and spatial distribution of γ rays.

9.1 Hot spots on the CTF vessel

Without yet making an attempt to understand the species present in the nylon film, we can observe that some regions of the CTF vessel are apparently more radioactive than others. It is worth taking a moment to discuss these hot spots. It should first be noted that in this chapter, the range of θ , the latitudinal coordinate in the spherical (r, θ, ϕ) coordinate system, is taken to be $-90^\circ < \theta < +90^\circ$, with $\theta = 0$ defining a great circle in the xy -plane (the CTF vessel “equator”). This convention is used in order to maintain the conceit of the CTF vessel as a globe having north and south poles at latitude $\pm 90^\circ$ and equator at latitude 0° . As in the previous chapter, the data used in this chapter come from Runs 2300–2563 unless stated otherwise.

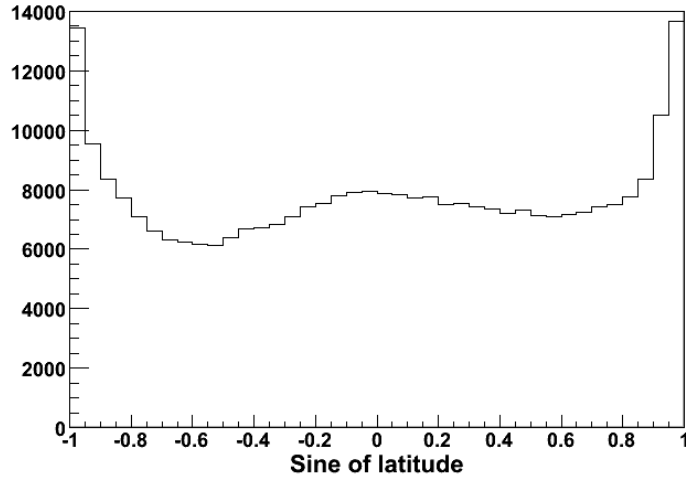


Figure 9.1: Histogram of the sine of the latitude of neutrino energy window events reconstructed in the range $80 \text{ cm} < r < 120 \text{ cm}$. Regions on a sphere bounded by circles of latitude whose sines differ by a constant amount have equal area. Thus a uniform distribution of surface events would produce a constant histogram. In this case, the histogram is mostly constant except for spikes at the south pole (left) and north pole (right), and a low-amplitude, broad bump near the equator (center). The bins of the histogram cover regions with $\Delta(\sin \theta) = 0.05$; therefore, each bin represents $1/40$ of the surface area of the CTF vessel.

Low-background detectors must be built with the utmost care in order to prevent radioactive contamination. For instance, an unknown mistake during construction of the acrylic vessel of the Sudbury Neutrino Observatory produced a hot spot nicknamed the “Berkeley blob,” a point-like source on the vessel with an activity equivalent to about $9 \mu\text{g}$ of ^{232}Th [171]. Though this hot spot had the serendipitous effect of providing a calibration source intrinsic to the SNO detector, its presence could have been problematic if SNO was intended to observe neutrinos at lower energy ranges. The CTF hot spots can tell us what to expect in the way of similar features on the Borexino Inner Vessel.

9.1.1 The north and south end regions

The most immediately obvious regions of higher radioactivity in the CTF are the north and south poles of the vessel. This is apparent in vertical cross-sections of the detector such as Figures 8.17a and 8.18a. We can also look directly at the distribution in θ of surface events. Selecting only those events in the neutrino window with a radial coordinate between 80 and 120 cm, we plot a histogram of the sines of their latitudes in Figure 9.1. It is easy to show that the region on a sphere bounded by two circles of constant latitude θ_1 and θ_2 has surface area $A = 2\pi r^2 |\sin \theta_1 - \sin \theta_2|$. Therefore, a uniform surface distribution should yield a constant-valued histogram. As seen in the figure, the histogram is fairly uniform between latitudes 55° S and 55° N ($\sin 55^\circ = 0.82$), but there are spikes at both poles.

The hotness of the poles comes as no surprise, since more material is present there (the two solid nylon end regions) than anywhere else on the vessel. Furthermore, there is evidence (described in the previous chapter, and in Section 9.2.2) that particulate material has settled at the south pole of the vessel, increasing the radioactivity further.

The average observed event rate per unit area during Runs 2300–2563, in the neutrino energy window (250–800 keV), is 75 events/day/m² for the north polar region ($\theta > 60^\circ$ N), 72 events/day/m² for the south polar region ($\theta < 60^\circ$ S), and 54 events/day/m² for the vessel film between 60° S and 60° N. These regions on the vessel have respective areas of 0.842, 0.842, and 10.88 m². The event rate includes events having a reconstructed radial coordinate between 80 and 120 cm; it therefore also incorporates a large number of internal events. Of course, it also cannot help but include many external γ -ray events. Nevertheless, the large difference between the quoted values shows that the poles are substantially more radioactive than the rest of the vessel film.

We may do somewhat better by subtracting away the estimated contribution due to internal events. From Section 8.5, we have an average value of 33 events/day in the innermost 65-cm radius (or one ton) of scintillator volume. The expected ratio between the numbers of

internal events with radial coordinates observed in the range 80–120 cm and in the range 0–65 cm is roughly 1.75, a figure obtained by performing the relevant integrals over the $f_d(r)$ function defined by Equation (5.48) and taking their ratio. (The value of the position resolution σ was assumed to be 15 cm, but using 10 cm instead changes the ratio only slightly.) This implies that the surface events are contaminated by internal events in the amount of $33 \text{ events/day} \times 1.75/12.56 \text{ m}^2 = 4.6 \text{ events/day/m}^2$. This is small compared to the overall surface rate. Subtracting off the value for internal events gives respective values for the north polar region, south polar region, and remainder of the nylon film of 70, 67, and 49 events/day/m²: the poles are at least about 40% hotter than the rest of the vessel.

If we consider these same values only during the period of lowest contamination in the scintillator, roughly Runs 2350–2447 (live time 213.4 days), we obtain respective values (corrected to subtract off internal events) for the north polar region, south polar region, and remainder of the nylon film of 71 events/day/m², 67 events/day/m², and 47 events/day/m². The average internal contamination in the neutrino energy window during this period is 25 events/day/ton rather than 33. Despite this decrease in internal contamination, the combined surface and external contamination observed seems to be fairly constant and stable.

9.1.2 Hot spots on the nylon film

As shown in Figure 9.2a, the radioactivity of the CTF nylon vessel in the neutrino energy window is non-uniform even far from the poles. There are three roughly circular hot spots located on the vessel equator, distributed more or less at equal distances around it. These hot spots were observed to remain constant in position over time. The figure has been corrected to exclude an estimated contribution due to internal events of 4.6 events/day/m².

Including the internal event subtraction, the hot spots have maximum amplitudes of 75–85 events/day/m², compared to the minimum (background) value seen of 30 events/day/m².

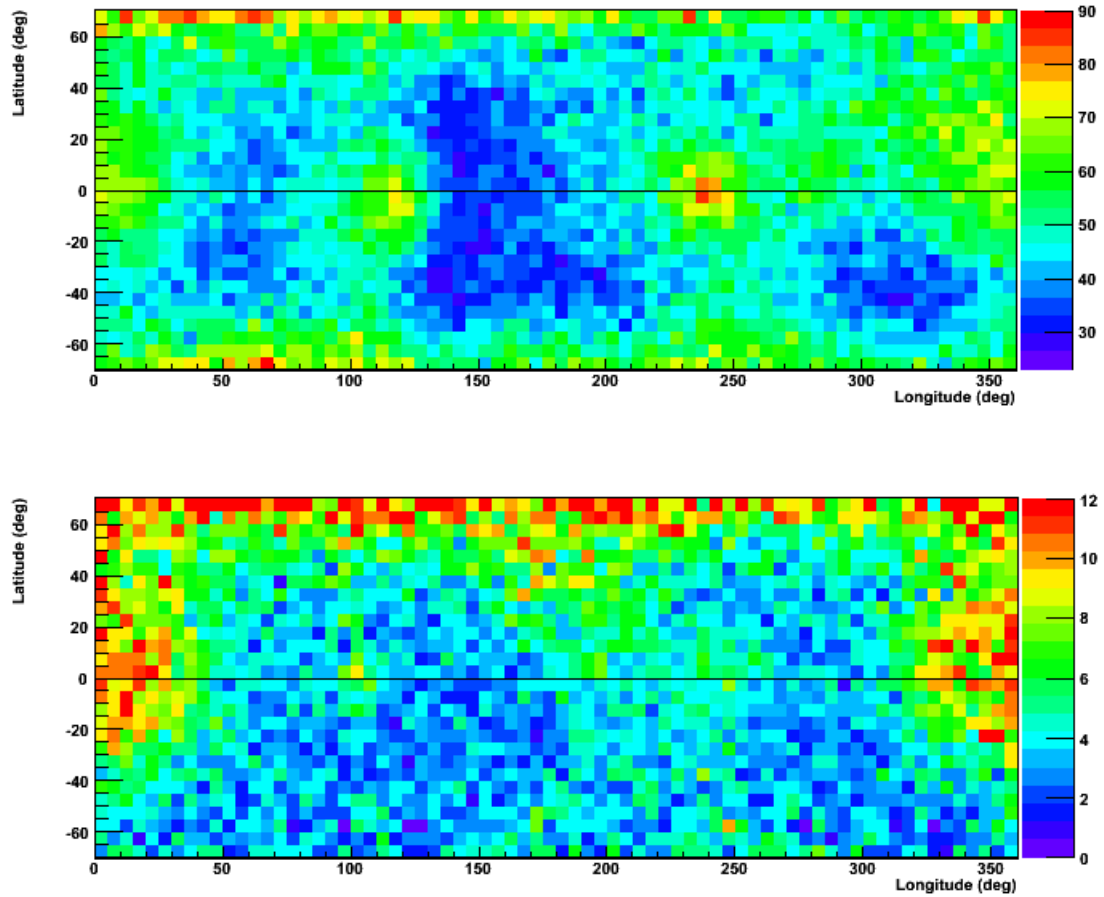


Figure 9.2: “Maps” of radioactive hot spots on the surface of the CTF vessel. Bins are 5° on each side, and the colors correspond to the event rate observed in each bin during Runs 2300–2563, in units of events/day/m². (Bins near the poles of course have different area than bins near the equator.) The data shown here include only events with reconstructed radial coordinates between 80–120 cm, and reconstructed latitudinal coordinates (θ) between -70° and $+70^\circ$. In addition, the constant internal event contribution has been statistically subtracted away, although it is small compared to the observed rate of surface events. The upper map (part a) shows events in the neutrino energy range, while the lower map (part b) is for events in the energy range 1.2–2.0 MeV. Note the suppressed zero of the color scale in the upper map; the two color scales differ. Most interestingly, the pattern of hot spots varies depending upon the energy range observed.

This is almost a factor of three difference! Without the hot spots, the average vessel surface contamination away from the poles would be 330 events/day in the neutrino energy window instead of the observed 510. The origin of these hot spots is unknown. A rough estimate of the activity of the most radioactive spot, at $\phi = 240^\circ$, yields about 12 events/day over the background value. This rate is similar to the figure of 0.7 events/hr (17 events/day) made public for SNO's hot spot [171]. However, it must be noted that the low energy threshold for SNO is 30 PMT hits, corresponding in the case of that detector to a several-MeV event, so the total rate of the SNO hot spot is probably much higher than the CTF hot spots. This represents at least a small triumph for the method of manufacture of the CTF vessel. In Borexino, the vessels were assembled in a yet more careful manner; some details are given in reference [44].

A similar map for higher energy events, 1.2–2.0 MeV, is shown in Figure 9.2b. Some equatorial hot spots are still present, but they do not precisely match up with those on the other map. This implies that different hot spots are produced by a different mix of radioactive isotopes, and therefore have different origins. The higher energy events also seem to be more prominent in the northern hemisphere, likely due to the greater number of γ rays produced by the bulkier north end-cap and pipe.

9.1.3 Attempts to observe the hold-down ropes

Recall from Chapter 6 that the CTF vessel, which is suspended in water but filled with less dense organic scintillator fluid, is held down against the buoyant force by 16 nylon monofilament lines. Since each of these lines is strung over the top of the nylon vessel and tied down at the bottom of the water tank on each end, 32 nylon lines cross the CTF equator in all, or two per panel of nylon film.

We may ask whether it is possible to see a pattern of events due to these lines. A pattern could also be seen due to the seams between the nylon film panels if the glue used was

sufficiently radioactive. In either case, the pattern should be most apparent in a histogram of the number of events in specific ranges of the longitudinal coordinate ϕ . Such a histogram is shown in Figure 9.3 for events with energies in the range 1.2–2.0 MeV (bracketing the 1.46 MeV ^{40}K electron capture photopeak and the 1.76 MeV ^{214}Bi γ ray). The events in this figure have latitudes between 60° S and 60° N, and radial coordinates between 80 and 120 cm. Though no pattern with a period of 11.25° ($360^\circ/32$) is apparent, the hot spots on the equator are quite obvious.

It is possible that the Fourier transform of this histogram is more informative. The unnormalized discrete Fourier transform of a histogram with N intervals numbered $j = 0, \dots, N - 1$ is defined by

$$Y_k = \sum_{j=0}^{N-1} X_j e^{-2\pi i j k / N}, \quad (9.1)$$

where X_j is the value for the j^{th} interval of the histogram. It is similar to the well-known continuous Fourier transform, but adjusted for the case in which only a finite amount of data is known. The k^{th} element of the result is a measure of the sinusoidal component of the original histogram which repeats k times over the histogram range.

The complex Fourier components Y_k for $k = 0, \dots, 50$ of the longitudinal histogram were calculated numerically using the FFTW software package [172], version 3.0.1. Their magnitudes $|Y_k|$ are shown in Figure 9.4. Note the logarithmic scale on the y -axis. The first maximum of the plot (after the constant component $k = 0$) is at $k = 2$, corresponding to the two most obvious hot spots on the equator. No significant maxima are seen afterward; in particular, the expected large peaks at $k = 16$ and $k = 32$ are not present.

If the nylon ropes do contribute significantly to the spectrum, either they are in too much disarray to contribute a periodic component, or they are sufficiently close together that the finite spatial resolution of the detector smears their signature to the point of invisibility in Fourier space. This latter possibility at first seems unlikely, since the average separation between ropes at the equator should be 19.6 cm, rather greater than the detector spatial

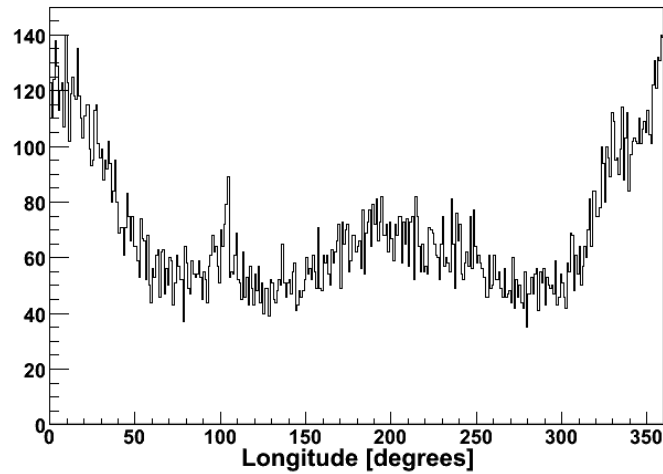


Figure 9.3: Histogram of events in the energy range 1.2–2.0 MeV as a function of longitude (the CTF ϕ coordinate). Bins are 1° of longitude wide. The events selected for inclusion had reconstructed radial coordinates between 80–120 cm, and reconstructed latitudinal coordinates (θ) between -60° and $+60^\circ$. The data are taken from Runs 2300–2563. The peaks of the graph correspond to the hot spots of the surface activity map in Figure 9.2b.

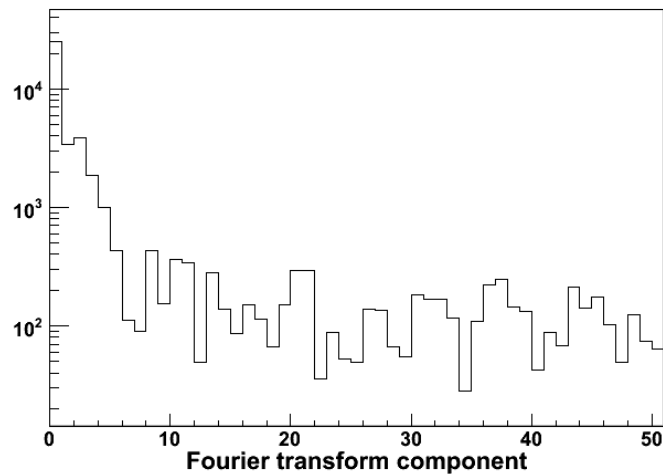


Figure 9.4: The discrete Fourier transform of Figure 9.3. Magnitudes are shown for Fourier components 0 through 50. Note the logarithmic scale on the vertical axis.

resolution. We must remember, though, that the ropes may only be observed via external γ rays entering the scintillator. The difficulty of reconstructing γ ray positions accurately, when they scatter multiple times at locations several cm apart, has already been mentioned. In any case, it is also quite probable that the ropes do not make a significant contribution to background; their total mass is very small.

9.2 Radon and thorium in or near the nylon film

We can search for heavy elements (the ^{238}U and ^{232}Th decay chains) on the nylon vessel in the same way as in the bulk of the scintillator: via the method of coincidences. The event loss due to geometric considerations, however, means that the method becomes unreliable for surface events. For more than $\frac{1}{4}$ of coincidences occurring on the inner surface of the nylon vessel, neither event in the coincidence will be detected. For another more than $\frac{1}{2}$, only one of the two events will be seen, implying that the set of supposed singles events is itself contaminated by coincidence events. (For instance, it is not necessarily true that the energy spectrum of α -like singles events is free of ^{214}Po or ^{212}Po .) Only in less than $\frac{1}{4}$ of cases can the full coincidence be detected. And this is the best-case scenario, for decays that occur on the inner surface of the nylon vessel, not embedded inside the nylon film. Any study of coincidences at the vessel surface must bear this fact in mind.

9.2.1 $^{214}\text{BiPo}$ coincidences and the implications for radon

We will use the same set of cuts defined in Section 8.2.1. In this case, we now consider all coincidences passing the cuts, not only those with a radial coordinate of less than 65 cm. Two basic phenomena may be studied with these data: the contamination of the nylon vessel film by uranium and radon, and the amount of light collected by the CTF as a function of the event radial coordinate.

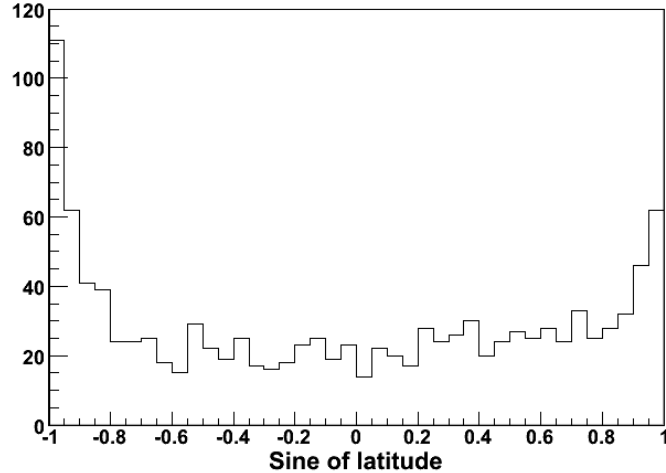


Figure 9.5: Histogram of the sine of the latitude of ^{214}Po events reconstructed in the range $80\text{ cm} < r < 120\text{ cm}$. A uniform distribution of surface events would produce a constant histogram. Here, the histogram is mostly constant except for spikes at the south pole (left) and north pole (right). The south pole is clearly more radioactive in ^{214}Po . Compare with the ^{210}Po distributions shown in Figures 8.17 and 8.18.

First, however, consider the distribution in θ of surface events. Selecting only those ^{214}Po events (from the $^{214}\text{BiPo}$ delayed coincidences) with a radial coordinate between 80 and 120 cm, we plot a histogram of the sines of their latitudes in Figure 9.5. As before, a uniform surface distribution should yield a constant-valued histogram. The histogram is indeed quite uniform between latitudes 55° S and 55° N ($\sin 55^\circ = 0.82$), but there are spikes at both poles. They indicate that, as with the total set of events in the neutrino window, there are concentrations of radon daughters near the top and bottom of the vessel. These may be indicative of several things. There could be leaks of radon entering from the two end pipes; the poles could be hotter due to the presence of the end pipes (and other masses of bulk nylon) themselves; or, as proposed before, particulate could have settled onto the bottom of the vessel. The last explanation seems perhaps the best one, given that the south pole has a higher amount of ^{214}Po than the north.

Radial distribution of the coincidences

In reference [42], D. Franco puts Equation (5.48), the expected distribution function $f_d(r)$ of internal events, to good use in fitting the radial distribution of ^{214}Po events from $^{214}\text{BiPo}$'s. The use of only the internal event distribution function was a reasonable simplification. In that case, the period under examination included Runs 2074–2090, which had a high internal radon contamination (over 100 $^{214}\text{BiPo}$ coincidences/day/ton).

During the recent period of Runs 2300–2563, the amount of radon in the detector was much lower, on the order of one coincidence/day/ton or less. Therefore, we have a reasonable hope of observing surface contamination by fitting the observed radial distribution of coincidences to the function

$$f(r) = N_i f_i(r; \sigma) + N_s f_s(r; \sigma), \quad (9.2)$$

where N_i is the number of internal events in a data sample, N_s is the number of surface events, and f_i, f_s are the functions of Equations (5.48) and (5.51), respectively. (For simplicity, we take σ to be a constant parameter of the model instead of a radially-dependent function.) Instead of using the radial coordinate of the average position of the two events, as in Section 8.2.1, we follow reference [42] and only use the radial coordinates of the ^{214}Po event; this avoids problems of reconstructing the γ -ray rich ^{214}Bi events near the vessel film. The free parameters of the fit are R , the CTF vessel radius; σ , the position resolution of the detector; and N_i , the number of internal events. R and σ are kept free since we do not know the precise shape of the vessel, nor the exact dependence of σ on the radial coordinate of an event. It is hoped that by letting them float, they will settle down to reasonable averaged values. The integral over $f(r)$ is required to be N , the total number of $^{214}\text{BiPo}$ coincidences, so N_s is constrained to equal $N - N_i$.

The set of coincidences meeting all the cuts includes 1099 ^{214}Po coincidence events. 197 of these were previously analyzed in Section 8.2.1. However, as one additional tweak to the analysis, all ^{214}Po events with a latitude coordinate θ whose absolute value is greater than

60° are excluded. (In other words, we exclude twin cones with apexes at the origin and symmetry axes on the z -axis.) This tweak removes from the data sample whatever may be the cause of the higher concentration of radon daughter events at the poles of the vessel, permitting us to consider only diffusion through the nylon film and emanation from it as sources of radon. The excluded region is shaped like a double cone, apexes at the vessel center, in order to keep the ratio of surface to volume included by the cut constant over all radii. The cut excludes only 13.4% of internal events if they are distributed homogeneously, so the statistics should not suffer. Once this volume cut is made, 787 candidate ^{214}Po events remain in the data sample (the excluded double cone volume thus contains 312 possible ^{214}Po events).

We now briefly consider the possibility of contamination of the data sample with accidental coincidences. If the time cut is relaxed to accept coincidences with delay times up to $\Delta t = 1000 \mu\text{s}$ instead of $500 \mu\text{s}$, there are 894 candidate coincidences instead of 787. A fit of the coincidence time for these 894 coincidences to an exponential decay curve (keeping the decay time constant fixed to the mean lifetime of ^{214}Po) plus constant term (Figure 9.6) yields an expected total of 951 ± 39 true $^{214}\text{BiPo}$ coincidences, and a value of -17 ± 19 accidental coincidences. The former value is consistent with the observed 787 events meeting the more restrictive time cut, divided by that cut's efficiency of 79.8% (resulting in 986 expected coincidences). The latter value gives an upper limit at 90% CL of 7 accidental coincidences in the range 20–1000 μs , or 3.5 accidental coincidences among the set of coincidences meeting the more restrictive time cut. This value, happily, is negligible.

The fit to the radial distribution, Equation (9.2), for the ^{214}Po events meeting all the cuts (including the volume cut and the more restrictive coincidence time cut) is shown in Figure 9.7. This fit yields a value of $9.3 \pm 1.4 \text{ cm}$ for σ , while the value of the vessel radius parameter R is found to be $112 \pm 4 \text{ cm}$. The unexpectedly large value of R may result from the distorted hot-air balloon shape of the vessel. The number of internal events was determined to be 653 ± 87 . Since the amount of scintillator in the CTF is 3.85 tons [169], and the volume cut excludes 13.4% of it, the number of observed internal events per ton

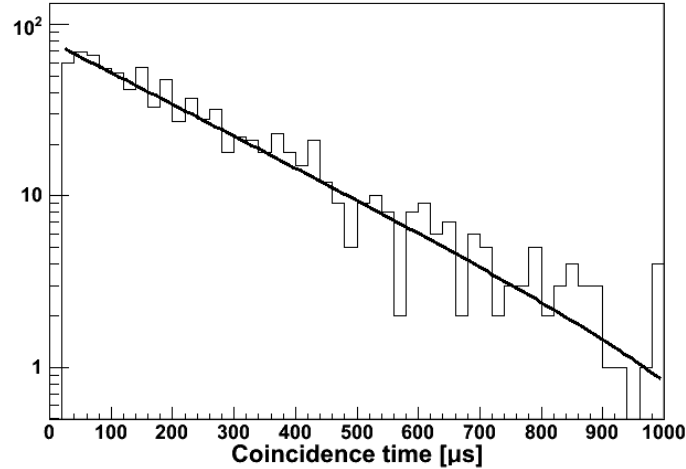


Figure 9.6: Histogram of the coincidence times for candidate $^{214}\text{BiPo}$ coincidences in Runs 2300–2563, with the double cone-shaped volume containing the vessel poles excluded. They were fit to an exponential decay plus constant term. Only candidates with $20 \mu\text{s} < \Delta t < 500 \mu\text{s}$ were used in the main analysis, although those having Δt up to $1000 \mu\text{s}$ are shown and fit in this histogram. The fit results give an expected total of 951 ± 39 true $^{214}\text{BiPo}$ coincidences, and a value of -17 ± 19 accidental coincidences with Δt in the range 20– $1000 \mu\text{s}$. The ^{214}Po mean life of $237 \mu\text{s}$ was kept fixed in the fit.

is 196 ± 26 . This is to be compared with the 197 events observed in the central 65-cm radius of scintillator; multiplying that value by the 65-cm radial cut scale factor of 1.073 yields 211 events/ton. The two values are consistent, implying that the internal $^{214}\text{BiPo}$ coincidences are distributed uniformly within the vessel.

The derived surface contamination of $N_s = N - N_i = 134 \pm 87$ events implies a surface event rate, extrapolated to the entire vessel surface, of 0.33 ± 0.22 events/day. [In the excluded volume, on the other hand, the number of surface events may be estimated as $(1099 - 787) - (196 \text{ events/ton} \times 3.85 \text{ tons} \times 13.4\%) = 211 \pm 26$, implying a rate per unit area ten times greater near the poles!] We may correct the overall surface event rate by the efficiency of the coincidence time cut, $\epsilon = 79.8\%$, to obtain 0.41 ± 0.28 surface events/day. The efficiencies of the other cuts used in detecting coincidences are not well-known for surface events. For instance, about half of the γ -ray emissions from ^{214}Bi decays near the

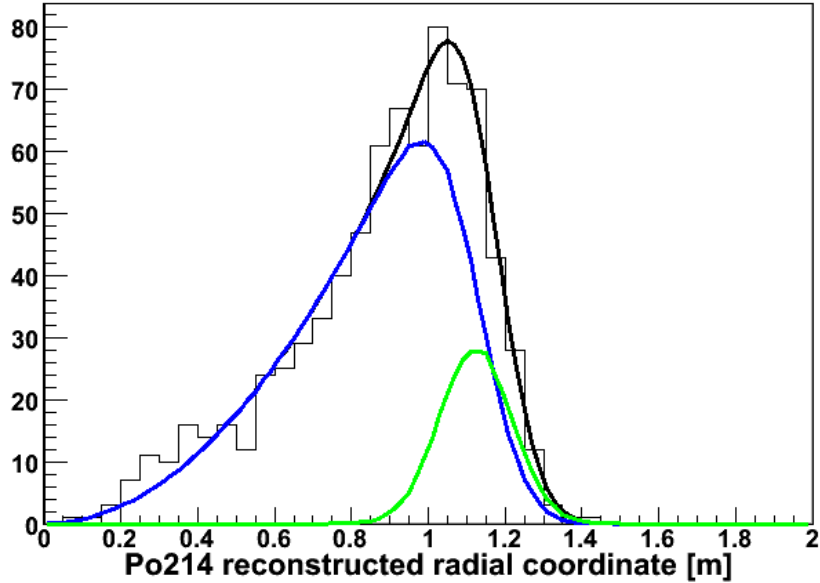


Figure 9.7: Distribution of the reconstructed radial coordinates of the ^{214}Po events in the 787 observed $^{214}\text{BiPo}$ coincidences within the volume cut during Runs 2300–2563. The black curve is the best fit to Equation (9.2). The blue and green curves represent the internal and surface components of the fit, respectively. They have respective integrals of 653 events and 134 events.

vessel surface are lost to the water buffer, which as shown below shifts the spectrum of that isotope to lower energies, decreasing the efficiency of that energy cut. Let us estimate their combined efficiencies at 85%; then the overall surface event rate becomes 0.48 ± 0.33 surface events/day.

Surface events may be attributed both to radon diffusing inward from the CTF water buffer, to radon emanation from radium atoms embedded in the nylon film, and to radioactive atoms adsorbed on the inner film surface. If we suppose that the CTF scintillator fluid does not exhibit convection, radon atoms from these sources will be present within a thin (few cm) boundary layer just inside the vessel. The thickness of this boundary layer is effectively zero, given the finite position reconstruction resolution. In the worst case, all observed events are from atoms on the inner surface of the vessel or in “dirt” attached to

it; in the best case, all radon atoms whose progeny we see have diffused into a boundary layer in the scintillator. (The fraction of coincidences detected that originate from atoms embedded *within* the nylon film will be much smaller than the total, due to the extreme short range of the α particle.) The figure of 0.48 events/day thus represents at least about $\frac{1}{4}$ of all surface events; the true value is presumably in the range 0–4.5 events/day at 2σ .

Following the discussion on radon in CTF 1 of Section 6.4.1, suppose that this event rate corresponds only to radon diffusion from the water buffer. The radon concentration in the external water implied by the surface coincidence rate has an upper limit of 75 mBq/m³, quite a bit higher than the known value for CTF 3. (Near the walls of the tank, the radon activity is about 30 mBq/m³; in water inside the shroud, it is more like 2 mBq/m³ [169].) On the other hand, if it results only from radon emanation of the nylon film, the ²²²Rn production rate in the film has an upper limit of 20 mBq/m³, similar to the value of 18.2 mBq/m³ measured for Sniamid nylon film. Recall that the CTF 3 film consists of C38F, not Sniamid; however, there is no reason to believe that the radioactive contaminant levels in the two materials would be quite different. It seems, then, that most of the surface radon in CTF 3 is probably produced by radon emanation from the nylon itself or by “dirt” adhering to the nylon film, rather than entering the scintillator via diffusion.

Light yield of events as a function of radial position

As mentioned above, the location of an event in the CTF vessel—energy of the event being taken as constant—has some effect on the number of photoelectrons detected. The most extreme cases are events whose energy spectrum includes a large number of γ rays, such as ²¹⁴Bi. For these events, the light loss is caused when a γ ray leaves the site of the event in a direction taking it out of the vessel into the water buffer. There it is invisible to the PMTs, as no scintillation light is produced. The probability of a γ ray escaping this way nears 50% for events near the vessel surface. Figure 9.8 shows the effect of such light loss on the ²¹⁴Bi spectrum.

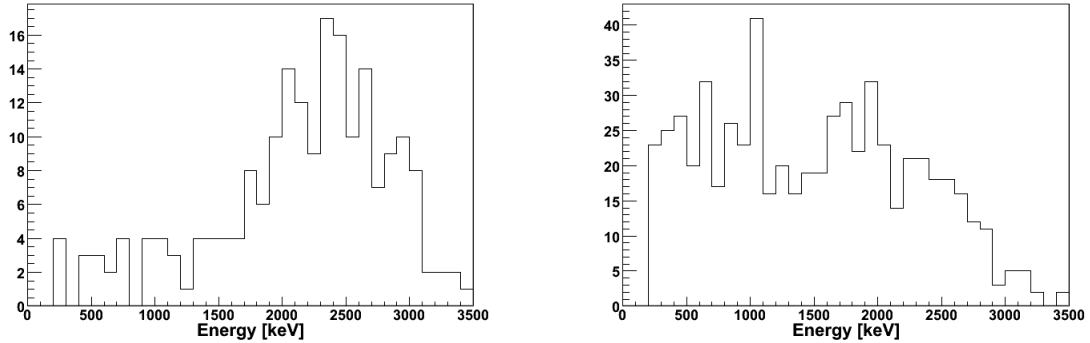


Figure 9.8: The energy spectrum of ^{214}Bi coincidence events in Runs 2300–2563. Both spectra are cut off below 200 keV by one of the coincidence energy cuts. In part (a), at left, the spectrum is shown for events with a radial coordinate $r < 65$ cm. It nicely matches the theoretical prediction shown in Figure 7.18a. (This plot is not perfectly identical to Figure 8.6a; in that case, the data sample was selected by the average position of *both* events in the $^{214}\text{BiPo}$ coincidences.) In part (b), at right, the spectrum is shown for events with a radial coordinate $r > 90$ cm. The spectrum at right has a much higher percentage of events with a low observed energy, as many of its γ rays are lost to the water buffer.

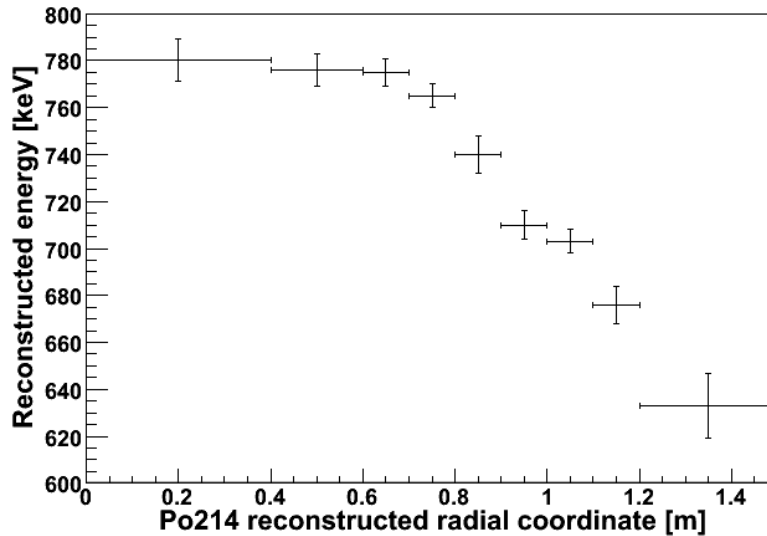


Figure 9.9: Reconstructed energy of the ^{214}Po α decay as a function of the reconstructed event radial coordinate. For $r < 70$ cm or so, the observed event energy is constant. Beyond that, up to 20% of the event light is lost. The reasons for the light loss are unclear.

Nevertheless, even events that produce no γ rays are affected to some extent. The energy peak of any monoenergetic α decay, for instance, appears to be at lower energies as the distance of the event from the detector center increases. To examine this phenomenon, we use ^{214}Po events once again. In order to obtain better statistics, the window of runs considered is expanded to Runs 2180–2563; runs toward the beginning of this period exhibit a high radon concentration due to the then-ongoing purification tests. ^{214}Po events are once again selected with the standard set of $^{214}\text{BiPo}$ coincidence cuts; the volume cut used earlier is now dropped. The mean energy of the ^{214}Po α peak as a function of radius is shown in Figure 9.9. Up to about 70 cm from the vessel center, it is fairly constant; beyond that, it decreases rapidly by 20%, from 780 keV down to 630 keV. It is also noteworthy that the width of the peak is defined by $\sigma_E \approx 60\text{--}70$ keV up to 80 cm, but beyond that the peak becomes significantly more broad, $\sigma_E \approx 90$ keV or more.

The cause of this phenomenon, which has also been described in reference [166], is not entirely clear. Somehow, light is being lost for events near the surface. It is possible that only events very near the vessel surface lose light, and the apparent light loss in the outer region of scintillator results from the fraction of true surface events that are erroneously reconstructed at those radial positions. This hypothesis would also explain the larger values of σ_E seen for the α energy peak near the vessel; they result from the overlap of the “normal” peak from internal events, and the lower-energy peak from surface events reconstructed in the wrong place. Perhaps the effect occurs as a result of light trapping, a consequence of the same total internal reflection of light that causes the “dark zones” described in Section 7.6.3. The dark zones have an inner radius of about 89 cm. However, the deformations of the CTF vessel from sphericity make this hypothesis seem unlikely. Alternatively, it may be simply that the reflectivity of the light cones attached to the PMTs is degrading, reducing the PMT efficiency for detecting photons that enter at a shallow angle. But if this was the case, we would expect the light yield function not to be so flat in the central region of the detector out to about 70 cm. No current hypothesis really seems to explain the light loss well.

Whatever the cause of the light loss near the surface of the CTF vessel, the effect is important to keep in mind when searching for peaks in the energy spectrum in that region.

9.2.2 $^{212}\text{BiPo}$ coincidences: evidence for thorium

To search for thorium, we use the $^{212}\text{BiPo}$ coincidences, detected with the same set of cuts defined in Section 8.2.2. Instead of having a 65-cm radial cut, we now look at the full data sample in Runs 2300–2563. A total of 637 candidate coincidences are observed. Of these, we expect that about 36 (only 5.6%) are internal events, judging by the observation of nine candidates within the central 65-cm radius of the detector in Section 8.2.2. Dividing by the time cut efficiency (the probability that a $^{212}\text{BiPo}$ pair has a coincidence time within the required 0.1–2 μs limits) of 78.4% yields an expected total of 813 $^{212}\text{BiPo}$ coincidences, both surface and internal, before taking the other cut efficiencies into account.

Consider what happens when the coincidence time cut is relaxed to include coincidences meeting all the other $^{212}\text{BiPo}$ cuts with $\Delta t < 5 \mu\text{s}$. We may fit a histogram of the coincidence time to an exponential decay curve plus constant term. In the fit, the decay time is fixed to that of ^{212}Po , 431 ns. The fit is made only to events having $200 \text{ ns} < \Delta t < 5 \mu\text{s}$; as seen in Figure 9.10, a significant fraction of coincidences with a coincidence time less than about 200 ns are lost. The results are a predicted number of 844 ± 39 $^{212}\text{BiPo}$ coincidences in total (matching the value of 813 obtained above), and a data contamination of 25 ± 12 accidental coincidences with delay times in the above range. From this we conclude that the number of accidental coincidences in the pool of candidate $^{212}\text{BiPo}$ coincidences with the more stringent time cut is about 9 ± 5 , or 1.4%.

The so-called accidental coincidences also include very fast $^{214}\text{BiPo}$ coincidences, as the ^{214}Po mean life is too long on this scale to distinguish their decay time distribution from a constant function. Statistically, the number of $^{214}\text{BiPo}$ coincidences included in the $^{212}\text{BiPo}$ sample should be 68.7% [energy cut] \times 2.5% [less restrictive time cut] times the 1099

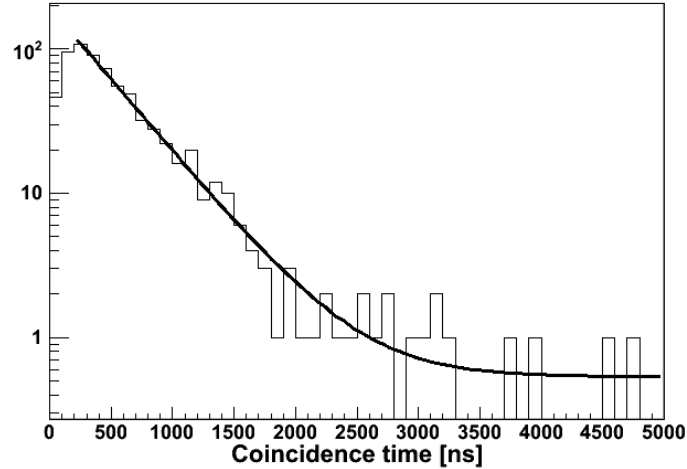


Figure 9.10: Histogram of the coincidence times for candidate $^{212}\text{BiPo}$ coincidences in Runs 2300–2563. They were fit to an exponential decay plus constant term. Only candidates with $100\text{ ns} < \Delta t < 2\text{ }\mu\text{s}$ were used in the main analysis, although those having Δt up to $5\text{ }\mu\text{s}$ are shown and fit in this histogram. The lower limit of the fit is at 200 ns due to an apparent inefficiency in the Group 2 trigger for faster coincidences. The fit results give an expected total of 844 ± 39 true $^{212}\text{BiPo}$ coincidences, and a value of 25 ± 12 accidental coincidences with Δt in the range $200\text{ ns} - 5\text{ }\mu\text{s}$. The ^{212}Po mean life of 431 ns was kept fixed in the fit.

coincidences observed in the previous section, or 19; this is consistent with the value of 25 ± 12 .

The energy spectrum of the ^{212}Po candidate events has a roughly Gaussian peak, shown in Figure 9.11. However, the lower-energy side of the peak exhibits some noise. It is not clear whether these events are really ^{212}Po shifted to lower energies by some effect, or some other species. Note that the data sample should be free of the $^{85}\text{Kr} \rightarrow ^{85\text{m}}\text{Rb} \rightarrow ^{85}\text{Rb}$ coincidences, whose first event is a β decay with a Q-value of only 173 keV . In any case, a Gaussian curve fit to the part of the spectrum above 700 keV has a peak value at $810 \pm 10\text{ keV}$ and a width defined by $\sigma = 112 \pm 7\text{ keV}$. This peak value is 18% lower than the predicted quenched energy of 989 keV , as might have been expected from the observed $\sim 20\%$ light loss for ^{214}Po events at the vessel surface.

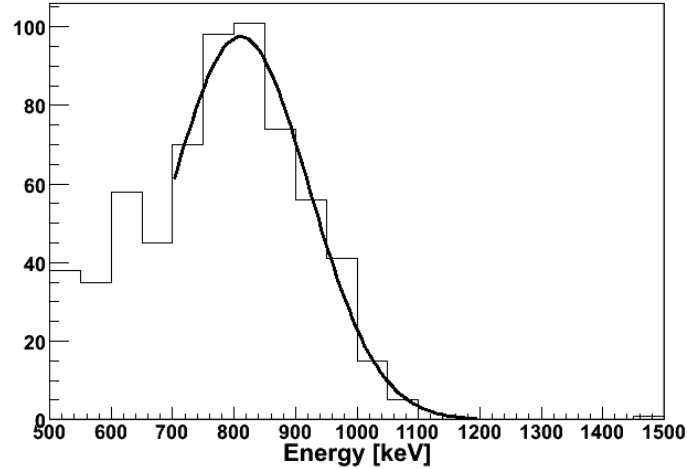


Figure 9.11: Energy spectrum of the ^{212}Po candidate events in Runs 2300–2563. The Gaussian curve shown, with a peak value at 810 keV, was only fit to the portion of the histogram above 700 keV. The origin of the lower-energy noise to the left of the Gaussian is not known.

Since we saw that about 5.6% of all the 637 observed $^{212}\text{BiPo}$ coincidence events are internal, while about 1.4% of them are actually accidental (including $^{214}\text{BiPo}$) coincidences, roughly 93% of all observed coincidences passing all cuts really are $^{212}\text{BiPo}$ coincidences at the vessel surface. The number of $^{212}\text{BiPo}$ surface events we expect is therefore about $93\% \times 844 \approx 785$ events, divided by the efficiency of the other cuts (we guess this to be again on the order of 85%) and the $^{212}\text{Bi} \rightarrow ^{212}\text{Po}$ branching ratio of 64%, and multiplied by the factor of four for the decay visibility. Assuming secular equilibrium, this gives an estimated total of about 5800 ^{232}Th decays on the vessel surface during the time period being analyzed.

In the 474 days of livetime covered by Runs 2300–2563, this number yields an event rate of about 12 thorium decays per day, or a total ^{232}Th mass on the inner vessel surface of 34 ng. (Compare to the thorium equivalent mass of $9 \mu\text{g}$ estimated for the SNO hot spot [171].) For comparison, such a mass of thorium evenly distributed through the scintillator fluid would correspond to $9 \times 10^{-15} \text{ g/g}$, much higher than the actual value of $(1.1 \pm 0.4) \times 10^{-16} \text{ g/g}$ derived in Section 8.2.2.

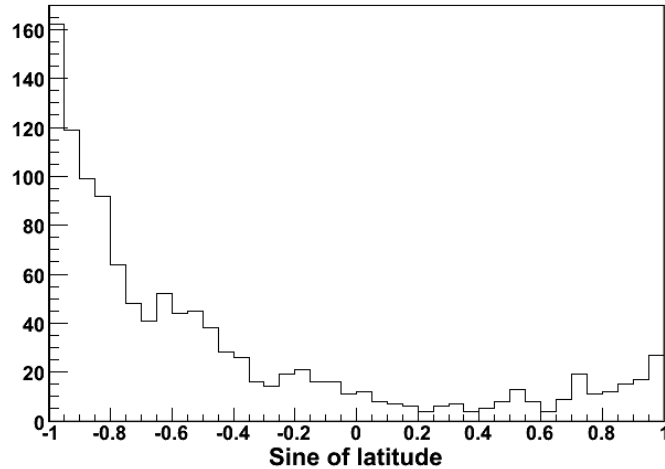


Figure 9.12: Histogram of the sine of the latitude of ^{212}Po events reconstructed in the range $80\text{ cm} < r < 120\text{ cm}$. If thorium were evenly distributed over the vessel surface, this histogram would be constant. This is far from the case; the vast majority of ^{212}Po events occur on the southern hemisphere of the vessel. Notice how broad the peak in the southern hemisphere is when compared with the corresponding peak in the ^{214}Po angular distribution, Figure 9.5.

If this mass of thorium were evenly distributed in the CTF nylon vessel film (total mass approx. 7.2 kg), the thorium contamination by mass would be 4.7 ppt. This is not far from the value of 3.9 ± 0.5 ppt obtained for C38F nylon film by Tama Chemicals in 1999 [12]. However, we must remember that the method of coincidences essentially sees only α particles produced in a thin skin of the nylon film closest to the scintillator, only a fraction of the total vessel mass. Thus the observed coincidence rate is in fact much higher than would be expected due solely to thorium contamination in the C38F nylon. This observation implies that most of the $^{212}\text{BiPo}$ coincidences have a source other than radioimpurities in the vessel material.

An even more suggestive finding is that the $^{212}\text{BiPo}$ coincidences are *not* evenly distributed over the vessel. (To measure their positions, we use only that of the better-defined ^{212}Po α decay.) A histogram of the sines of the latitudes of candidate events (Figure 9.12) shows that

the vast majority of them occur on the southern hemisphere of the vessel. This is much different from the case of $^{214}\text{BiPo}$ coincidences (Figure 9.5), which are largely uniformly distributed over the vessel surface area except for peaks at either pole of the vessel. The pattern seen in the $^{212}\text{BiPo}$ distribution by latitude strongly suggests that a layer of thorium-rich material has settled down to the bottom of the nylon vessel. This pattern has been confirmed independently in other analyses such as reference [166]. It is nice to see an independent confirmation, outside the ^{210}Po data, of a probable consequence of particulate falling out from the volume of scintillator.

The difference in shape between the radon and thorium surface distributions seen in Figures 9.5 and 9.12 also implies that, if the radon distribution results from particulate as well, the two sets of particulate have significantly different properties. The peak in this histogram at the south pole is much broader than the analogous peak in the sample of $^{214}\text{BiPo}$ coincidences. This suggests that most of the $^{214}\text{BiPo}$ coincidences belong to the same population as the ^{210}Po coincidences in the vertical column described in Section 8.3.5. These atoms are distributed in a fairly narrow column along the z -axis, from which material would be deposited only very close to the vessel south pole, rather than all across the southern hemisphere of film surface as for the ^{212}Po atoms.

9.3 ^{210}Po on the vessel

We analyze the ^{210}Pb daughter ^{210}Po for Runs 2190–2346, a period which begins immediately after the second silica gel column test, and ends more than a year before the appearance of the vertical column of events in the scintillator. The reason for this selection of events is that the surface events are easy to disentangle from internal events only if a more-or-less uniform distribution of internal events can be assumed.

For each block of approximately 10 runs in this period, the number of ^{210}Po events was estimated by accepting only events having an α/β discrimination parameter $\gamma_1^* < 0$ (91.2%

estimated cut efficiency). Candidate events were restricted to have reconstructed radial coordinates in the range 80–120 cm. The energy spectrum of these events between 200–800 keV was fit to the sum of a Gaussian curve and an exponentially decaying curve. The integral under the Gaussian was divided by the estimated α/β cut efficiency to yield the total number of ^{210}Po events within the radial cut for each time period. In order to have greater sensitivity to the presence of the Gaussian curve, its mean and width were fixed to specific values in each fit, defined below, instead of being allowed to float.

Meanwhile, for each set of about 10 runs, the number of ^{210}Po events seen within a 65-cm radial cut was multiplied by the 65-cm radial cut scale factor (1.073) and by the ratio (1.75) of the numbers of events expected to be reconstructed within the respective ranges $r < 65$ cm and $80 < r < 120$ cm. (The raw numbers of ^{210}Po events seen within the 65-cm radial cut were determined as described in Section 8.3.3, and plotted in Figure 8.13.) This value, the predicted number of internal events within the 80–120 cm radial cut, was subtracted from the corresponding number described in the previous paragraph, giving the estimated number of ^{210}Po surface events.

Due to this convoluted procedure required to extract the number of ^{210}Po surface events, it was not feasible to create a histogram of the ^{210}Po events as a function of $\sin\theta$ of the event, or a map of the surface distribution of the ^{210}Po events. One can create such plots for “ ^{210}Po -like” events meeting the cuts $200 < E < 550$ keV and $\gamma_1^* < 0$. However, these plots incorporate a fairly large number of other species as well, and can therefore be misleading.

Earlier sections in this chapter have shown that the CTF vessel end cap region tends to be much hotter than the rest of the nylon vessel. It is therefore worthwhile to divide up the surface into four regions: the two polar regions, with latitudes $|\theta| > 60^\circ$, and two equatorial regions, with latitudes $-60^\circ < \theta < 0^\circ$ and $0^\circ < \theta < 60^\circ$. The surface areas of the polar regions are each 0.842 m^2 , and those of the equatorial regions are each 5.44 m^2 . In the spectral fits of the energy histograms to a Gaussian curve plus exponential decay curve, the Gaussian mean and σ were kept fixed, with different values for each region:

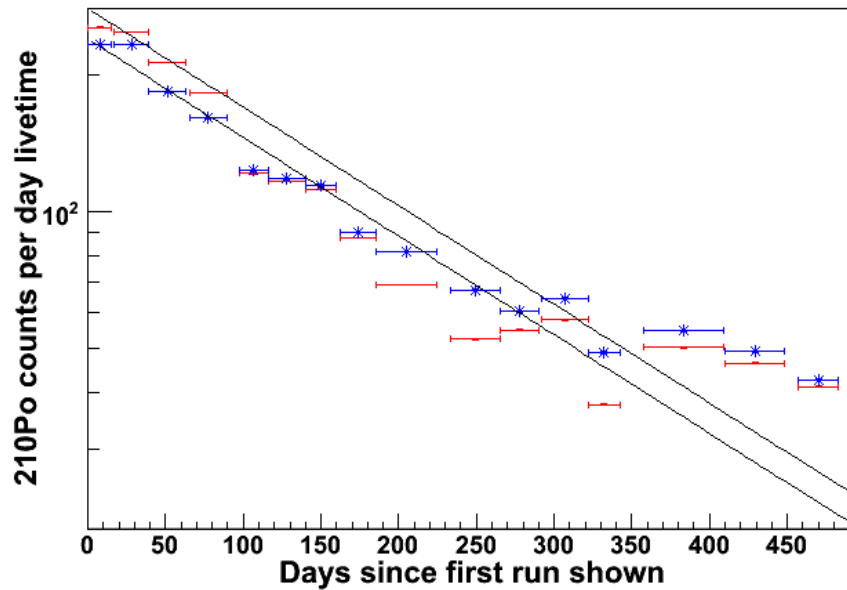


Figure 9.13: The decay of surface ^{210}Po on the CTF vessel. The graph covers the same period as Figure 8.14, and each data point represents about ten runs. Internal contamination has been statistically subtracted away to produce this plot. The blue (asterisked) data points represent the number of ^{210}Po surface events in the northern hemisphere, between latitudes 0° and 60° N. The line drawn through them is an exponential decay curve with the mean lifetime of the isotope and an initial activity of 240 events/day. The line is not a fit (it is drawn for illustrative purposes only) but nevertheless matches the data nicely. The red (not asterisked) data points, on the other hand, represent ^{210}Po surface activity in the southern hemisphere (latitudes between 0° and 60° S). Another exponential curve with the mean life of ^{210}Po has been drawn through the first four points (its initial activity is 280 events/day), but after that the southern surface activity declines rather faster than the expected decay curve. This behavior is quite puzzling. Nevertheless, both curves reach an eventual plateau of about 40 events/day, or 7 events/day/m².

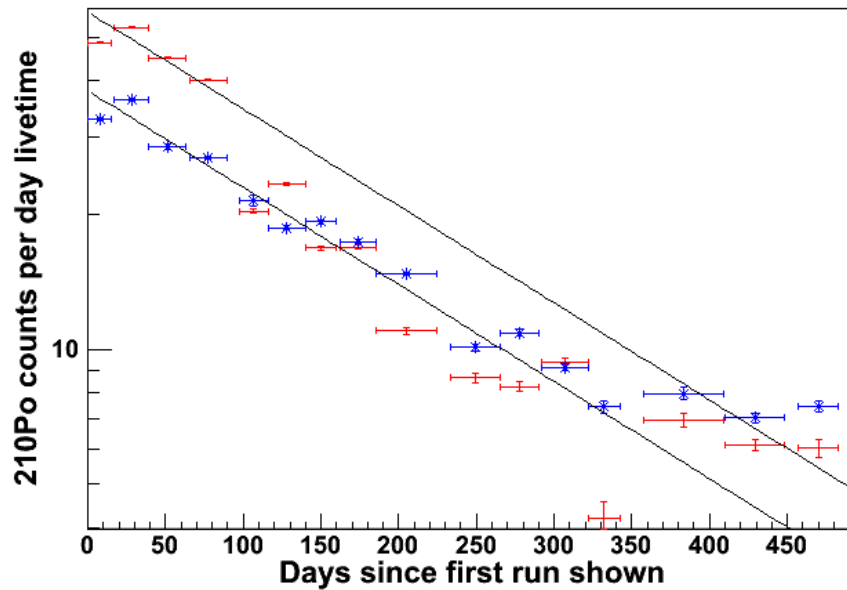


Figure 9.14: The decay of surface ^{210}Po near the north and south poles of the CTF vessel. This graph was constructed in the same way as Figure 9.13. The blue (asterisked) data points represent the number of ^{210}Po surface events near the north pole, above latitude 60° N. The line drawn through them is an exponential decay curve with the mean lifetime of the isotope and an initial activity of 38 events/day. The red (not asterisked) data points represent ^{210}Po surface activity near the south pole. An exponential curve with the mean life of ^{210}Po and an initial activity of 57 events/day has been drawn through the first four points, but afterwards the south pole activity declines much faster than the expected decay curve. Both curves reach an eventual plateau of 6–7 events/day, or 7–8 events/day/m².

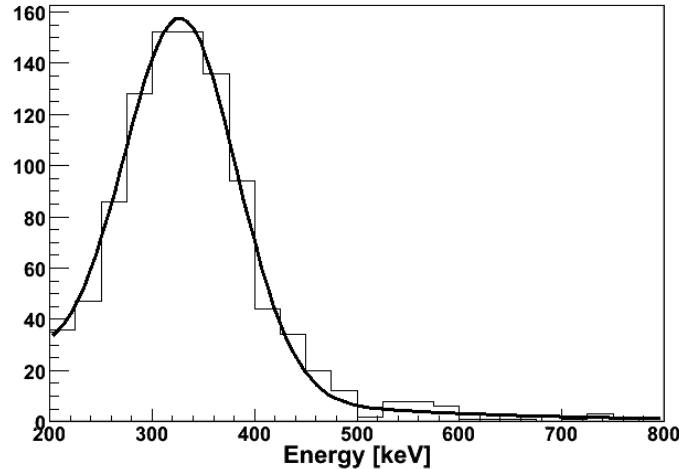


Figure 9.15: A typical spectral fit to the ^{210}Po peak (Gaussian peak plus exponentially decaying background). This fit is for Runs 2200–2209, for events near the south pole of the CTF vessel. The number of events in the Gaussian peak is given by the fit as 801, and in the exponential background (within the range of the histogram) as 172.

- North polar region: $\bar{E} = 311 \text{ keV}$, $\sigma_E = 68 \text{ keV}$
- North equatorial region: $\bar{E} = 343 \text{ keV}$, $\sigma_E = 56 \text{ keV}$
- South equatorial region: $\bar{E} = 341 \text{ keV}$, $\sigma_E = 55 \text{ keV}$
- South polar region: $\bar{E} = 328 \text{ keV}$, $\sigma_E = 55 \text{ keV}$

These values were obtained by first allowing the parameters to float freely in fits of the first four data points (having the highest ^{210}Po activities) for each region. From the results of the light loss study on ^{214}Po , it is no surprise that the mean value of the ^{210}Po peak for surface events is about 15% less than the predicted quenched energy of 396 keV. The additional 5–10% light loss in the polar regions is most likely due to the opacity of the end caps. A typical spectral fit is shown in Figure 9.15.

The results of this analysis of surface polonium may be seen in Figures 9.13 and 9.14. The calculated ^{210}Po contamination in the two northern hemisphere regions (blue) closely

follows the expected decay curve, with a mean lifetime of 200 days, for almost 300 days. After that, the curves plateau out to a constant value. In the two southern hemisphere regions (red), the contamination follows an exponential decay curve of the expected mean life for a short time (the first four data points, or 100 days). Afterwards, however, the number of ^{210}Po events in both data sets drops much faster than the isotope mean life. Despite this odd behavior, the southern hemisphere data also eventually reach constant plateaus. The equatorial regions tend towards constant values of 40 events/day, while the polar regions go to plateaus of about 6–7 events/day. These values all correspond to about 7 events/day per m^2 of nylon vessel inner surface.

These results have two surprising features. First, contrary to the pattern seen for other isotopes, the equilibrium contamination (eventual constant value) of ^{210}Po near the poles does not appear to be significantly higher than at other regions of the vessel. We may attribute this fact to the long lifetime of its progenitor ^{210}Pb : high radon levels near the two poles do not immediately translate into enhanced ^{210}Po concentrations. Instead, it seems that the surface of the nylon vessel is more or less uniformly covered with ^{210}Pb which eventually decays into ^{210}Bi and ^{210}Po at an approximately constant rate. This rate, a total of about 90 events/day over the entire inner surface, is to be compared with the observed ^{214}Po surface event rate of 0.33 ± 0.22 events/day. (Technically the former rate should be doubled, and the latter quadrupled, to take into account the geometric visibility factors.) The great disparity between the two rates means that the ^{210}Pb adhering to the vessel could not have originated from any source of radon in the CTF, but instead must have been carried in, for instance from contamination in the lines during scintillator filling.

The static nature of this contamination means that an adsorption equilibrium coefficient between nylon and pseudocumene may be deduced: $k = S/Y$, where Y is the internal contamination (per unit volume) and S is the surface contamination (per unit area) of ^{210}Po . The minimum internal rate of ^{210}Po was 1.6 ± 0.6 events/day/ton (from Section 8.3.4), or $Y = 1.4 \pm 0.5$ events/day/ m^3 . When we double the observed surface contamination of 7 events/day/ m^2 to account for the geometric visibility factor, we obtain a value for k

(within about 50%) of 10 m. This is much greater than the value of 1.2 cm determined in a small-scale laboratory experiment [46], so we may conjecture that the two populations of ^{210}Po in the CTF are very far from reaching equilibrium. At equilibrium, a much greater amount of ^{210}Po should be present in the bulk of the scintillator. This further supports the hypothesis of little or no convective mixing in the scintillator fluid.

The second surprising feature is the transient period during which the two southern hemisphere regions of the CTF vessel lose their ^{210}Po contamination faster than the isotope can decay. This occurs roughly during the same period in which the internal ^{210}Po contamination falls faster than expected. This observation seems contradictory to the hypothesis of Section 8.3.3 that the fast rate of ^{210}Po decay seen within the central ton of scintillator was due to particulates falling out onto the vessel bottom. If that hypothesis was true, we would expect to see surface contamination on the southern part of the vessel increase with time, or at least decrease more slowly than the isotope's characteristic decay curve. Unfortunately we do not have a good model to explain these observations of surface decay; they currently remain one of the many mysteries of the CTF detector.

9.4 External gamma rays

Up to this point, a significant contribution to the CTF event rate has been mentioned only in passing. A large number of events in the CTF scintillator actually originate from γ rays produced outside the nylon vessel. These γ rays may travel dozens of cm in water or pseudocumene before being fully absorbed; the mean distance traveled by a 1.5 MeV γ in pseudocumene before it is scattered the first time, for instance, is 15–20 cm.

In this section, for specificity we investigate mainly the ^{40}K 1.46 MeV and ^{214}Bi 1.76 MeV γ rays. ^{214}Bi γ ray events detected in the CTF with an energy of about 1.76 MeV are almost guaranteed to have originated from the external water buffer. As seen in Figure 9.8a, the probability of seeing an internal ^{214}Bi decay with that specific energy is fairly small;

generally the energy of the electron emitted in the β decay is also seen. The probability that such an internal decay is in the pool of single events (not detected as a coincidence) is even smaller, due to the $^{214}\text{Bi} \rightarrow ^{214}\text{Po} \rightarrow ^{210}\text{Pb}$ chain. Finally, the rate of ^{214}Bi decays within the scintillator is already quite low, only a few per day. On the other hand, we are not guaranteed that a particular ^{40}K γ ray came from an external event. There very well may be internal potassium contamination. The ^{40}K decay by electron capture produces only the γ ray, with no additional particles to change the observed decay energy when the decay happens within the scintillator.

9.4.1 The spatial distribution of external γ rays

The spatial distribution of events in the CTF caused by a particular type of γ ray may be calculated in three ways. As mentioned in the introduction of this chapter, it may be approximated analytically by a crude derivation, or estimated through Monte Carlo simulations. With these two methods we will assume, for simplicity, that the source of all external ^{40}K γ rays is the nylon film of the CTF vessel. A third method is to use the observed distribution of one species of γ ray, and extrapolate it to another of similar energy. Below we will calculate, for each method, the fraction of external ^{40}K electron capture events expected to be reconstructed between distances r_i^{\min} and r_i^{\max} , for each of the radial cuts i defined in Section 8.5.2.

The simplistic approximation

Assume a very naive model of γ ray interaction with matter, as developed in Section 5.5.2, in which all the energy of each γ ray is deposited at the point where it first interacts with the scintillator. From Equation (5.57), in this model we expect that the fraction of surface γ ray events reconstructed to lie between distances r and $r + \delta r$ from the detector center

should be equal to

$$f(r) \delta r \equiv \frac{1}{\sqrt{2\pi}} \frac{r \delta r}{\sigma \lambda R} \int_0^R dr' \left[\text{ei} \left(-\frac{R+r'}{\lambda} \right) - \text{ei} \left(\frac{r'-R}{\lambda} \right) \right] e^{-\frac{r^2+r'^2}{2\sigma^2}} \sinh \frac{rr'}{\sigma^2}. \quad (9.3)$$

The values R , σ and λ are parameters of the model. For the CTF, $R = 1$ m, and we suppose that σ and λ , the detector position resolution and γ ray attenuation length, respectively, are about 12 cm and 20 cm. This function, when integrated in r numerically over the radial cuts defined in Section 8.5.2, yields the following values:

- For region Ia ($r < 39.7$ cm): $\int f(r) dr \approx 0.00166$
- For region Ib ($39.7 \text{ cm} < r < 50.0$ cm): $\int f(r) dr \approx 0.00298$
- For region I ($r < 50.0$ cm): $\int f(r) dr \approx 0.00464$
- For region II ($50.0 \text{ cm} < r < 63.0$ cm): $\int f(r) dr \approx 0.01124$
- For region III ($63.0 \text{ cm} < r < 72.1$ cm): $\int f(r) dr \approx 0.02163$
- For all $r \geq 0$: $\int f(r) dr \approx 0.45$

Graphs of this reconstructed radial function $f(r)$ and the actual radial function $f_r(r)$ from which it is derived are shown in Figure 9.17a.

Monte Carlo simulations

For the Monte Carlo approximation, we simulate a uniform set of 1.46 MeV γ rays emitted isotropically from one point of the CTF nylon vessel. (It is only necessary to consider a single point source, since we are looking at radial distributions.) Each γ ray is followed on its path through water or scintillator until completely absorbed. Only those which deposit more than 95% of their energy (1.387 MeV) within the scintillator are considered further.

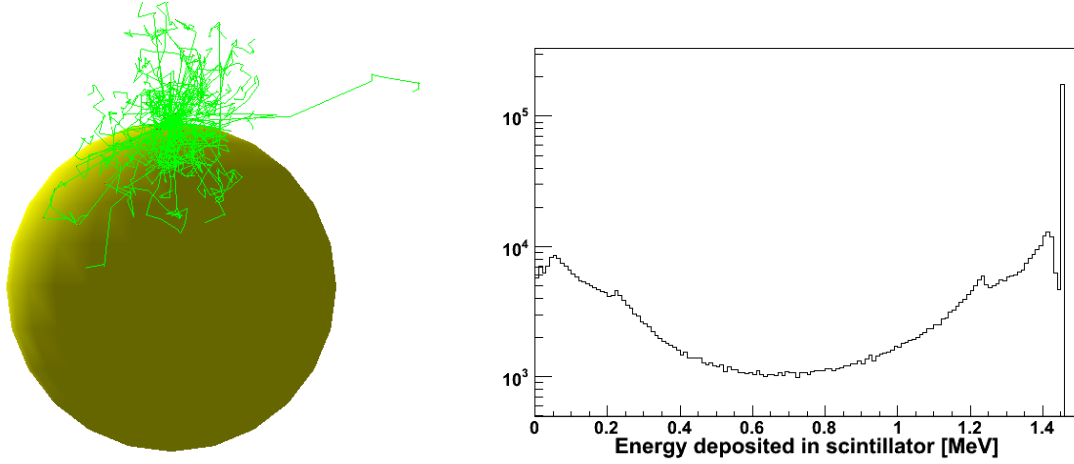


Figure 9.16: Monte Carlo simulation of the behavior of ^{40}K electron-capture γ rays originating on the vessel surface in the CTF. At left (part a) is a diagram of the trajectories of 100 of these simulated γ rays. The image is a projection onto the xz -plane, so some of the trajectories that appear to remain within the volume of scintillator actually are leaving it out of the plane of the page. At right (part b) is a histogram of the amount of energy deposited within the scintillator by each of 10^6 simulated γ rays. From left to right, readily apparent features of the simulated energy spectrum are the back-scatter peak (50 keV), Compton edge (1.4 MeV), and photopeak (1.46 MeV). The spectrum shown does not include the effects of the finite CTF energy resolution, which would tend to smooth out these features. Note that the y -axis is logarithmic.

Consider a simulated γ ray which deposits energy E_i at N different locations \mathbf{x}_i within the scintillator. Its “center-of-light” is defined to be

$$\bar{\mathbf{x}} \equiv \frac{\sum_{i=1}^N E_i \mathbf{x}_i}{\sum_{i=1}^N E_i}. \quad (9.4)$$

The histogram of the radial coordinates of all such centers-of-light is taken to represent $f_r(r)$, the radial distribution function of the event’s “position.” (The word “position” is within quote marks here due to its ill-defined nature for external γ ray events.) As in Section 5.5.2, we presume that the result of position reconstruction is to randomly reposition the center-of-light by convoluting its radial probability distribution function with a Gaussian function, yielding the reconstructed distribution function in r ,

$$f_d(r) = \frac{r}{\sqrt{2\pi\sigma^2}} \int_0^R dr' \frac{f_r(|r'|)}{r'} e^{-\frac{r^2+r'^2}{2\sigma^2}} \sinh \frac{rr'}{\sigma^2}. \quad (9.5)$$

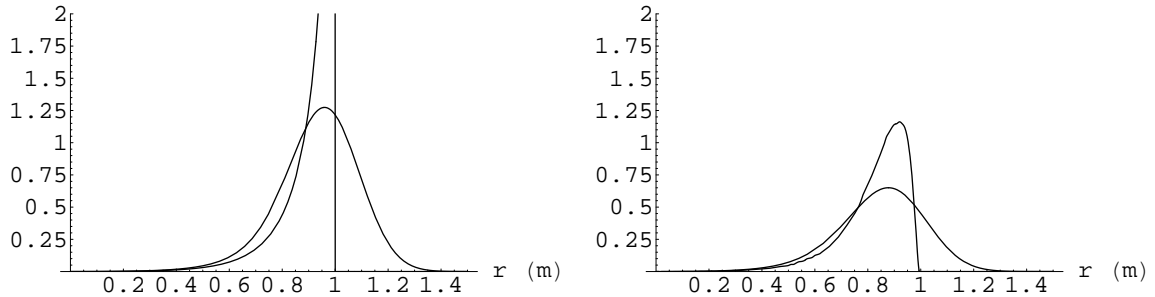


Figure 9.17: Two models of the radial distribution function of the center-of-light of ^{40}K electron-capture γ rays originating at the surface of the CTF nylon vessel. The center-of-light is defined in Equation (9.4) to include only energy deposits made by the γ ray within the scintillator. In each plot, the sharper peak represents the actual radial positions $f_r(r)$ of the simulated centers-of-light for the γ rays. The broader peak is the predicted radial distribution function $f(r)$ of their reconstructed positions, calculated by convolution of the actual distribution function with a Gaussian resolution function of $\sigma = 12$ cm. At left (part a), these functions are shown for the naive model in which all the energy of each γ ray is deposited at one point, with a mean γ ray travel distance of $\lambda = 20$ cm. At right (part b), these functions are shown for a simulation made with the GEANT 4 Monte Carlo libraries of one million γ rays.

This assumption is slightly flawed. It would be a good assumption if the CTF reconstruction software only used the pattern of PMT hits to determine the location of an event. However, the reconstruction software also uses knowledge of the timing of the event. The different energy deposits made by the γ ray occur at different times as the photon is scattered around. A better simulation would also incorporate the scintillation light produced at each γ ray point of scattering, as well as the PMTs, and simulate the hit times registered by each TDC of the detector; these values would be fed into the reconstruction software as if they were real data. Such a complete simulation of the CTF detector would be a much more complicated undertaking than the present Monte Carlo.

The present simulation was done with GEANT 4, version 8.0 [173]. One million 1.46-MeV γ rays were generated, originating at the north pole of a 1-m radius sphere of pseudocumene suspended in water, and given randomly chosen isotropic momenta. They were tracked, and

for those that deposited more than 1.387 MeV of energy within the scintillator, a histogram was constructed of the radial positions of their centers-of-light. This histogram, $f_r(r)$, is shown in Figure 9.17b, together with the predicted reconstructed distribution function $f(r)$ after convolution.

In the simulation, 65.6% of the γ rays deposited at least a little energy within the scintillator (Figure 9.16). However, only 25.4% of them deposited at least 95% of their energy in the pseudocumene. Even so, the photopeak in the simulated energy spectrum was still very sharp, far more prominent than any other feature in the spectrum.

When the function $f(r)$ constructed using this model was numerically integrated over the radial cuts defined in Section 8.5.2, the following values were obtained:

- For region Ia: $\int f(r) dr \approx 0.00258$
- For region Ib: $\int f(r) dr \approx 0.00479$
- For region I: $\int f(r) dr \approx 0.00737$
- For region II: $\int f(r) dr \approx 0.01727$
- For region III: $\int f(r) dr \approx 0.02756$
- For all $r \geq 0$: $\int f(r) dr \approx 0.25$

The ^{214}Bi 1.76 MeV γ ray

For reasons mentioned above, we expect that the observed ^{214}Bi 1.76 MeV γ -ray peak is produced only by external events. Because the energies and stopping distances of this γ ray and the 1.46 MeV ^{40}K γ ray in pseudocumene are similar, the amplitudes of this peak within the different radial cuts provide an approximation to the values of $\int f(r)dr$ for external ^{40}K events. These values are therefore given roughly by the following, tabulated earlier in Table 8.9, although the normalization constant k is unknown:

- For region Ia: $\int f(r) dr \approx 65k$
- For region Ib: $\int f(r) dr \approx 94k$
- For region I: $\int f(r) dr \approx 159k$
- For region II: $\int f(r) dr \approx 223k$
- For region III: $\int f(r) dr \approx 215k$

For specificity we will take $k = 6.45 \times 10^{-5}$, so that the integral of $f(r)$ over regions I and II matches the value of 0.02464 obtained in the Monte Carlo simulation.

9.4.2 Determining the internal ^{40}K contamination

In order to determine the internal ^{40}K contamination, we assume that the observed numbers of events in the photopeak in each of the radial cuts of Section 8.5.2 correspond to the sum of internal and external event spatial distributions. The internal distribution is supposed to be uniform over internal volumes (except near the vessel, due to edge effects which may be ignored here). The spatial distribution of γ rays produced by external events is more difficult to determine. As above, let the fraction of external ^{40}K photopeak γ -ray events reconstructed to lie within the radial shell $[r, r + \delta r]$ be $f(r) \delta r$. Then, for each radial cut i , the rate of events R_i seen within the cut is

$$R_i \equiv N_i/t = \mathcal{A}V_i + R_{\text{surface}} \int_{r_i^{\min}}^{r_i^{\max}} dr f(r). \quad (9.6)$$

In this equation, t is the livetime, V_i is of course the volume (or perhaps, depending on the units in which \mathcal{A} is desired, the mass) of the cut, and R_{surface} is the total rate of ^{40}K γ decays on the vessel surface. (Only 45% of these decays are actually seen in the scintillator.) The values of $\int_i dr f(r)$ for each of the three models under consideration, in each of the radial cuts, have already been calculated above.

External event distribution	External only		External + internal		
	R_{surface} [ev/day]	$\chi^2/(4-1)$	R_{surface} [ev/day]	\mathcal{A} [ev/day/ton]	$\chi^2/(4-2)$
Naive	48.5 ± 4.4	3.19	25.2 ± 8.8	0.80 ± 0.26	0.08
Monte Carlo	36.3 ± 3.2	1.82	21.2 ± 7.5	0.67 ± 0.30	0.10
^{214}Bi data	$51.6 \pm 4.6^*$	3.17	$55.4 \pm 29.5^*$	-0.11 ± 0.84	2.37

Table 9.1: Fit to the rate of ^{40}K electron capture decays on the vessel surface and in the CTF scintillator, using the three models for external event distribution described above. The data points used were for the four regions Ia, Ib, II, and III (the regions were defined in Section 8.5.2). The columns headed “External only” give the fit results when only an external contribution is assumed; those labeled “External + internal” are the results of fits to the full Equation (9.6). The asterisked values in the row for ^{214}Bi data are based on the assumption that the normalization constant k defined previously is equal to 6.45×10^{-5} .

These data have been fit to Equation (9.6) using the numerical integrals over $f(r)$ obtained for each of the three methods. The results are presented in Table 9.1, along with the results from a fit only to an external background [$R_i = R_{\text{surface}} \int_i dr f(r)$]. The errors shown in the fit results reflect only the errors reported in Table 8.9 for the numbers of ^{40}K γ events, originating with the energy spectral fits, not any systematic errors in any of the methods.

The results of Table 9.1 are technically consistent within the errors quoted, but they have rather different implications. Use of the ^{214}Bi γ ray peak to represent the presumed radial distribution of external ^{40}K γ rays (last row of the table) implies only an upper limit on the internal ^{40}K contamination. This limit is 0.73 events/day/ton at 1σ , corresponding to an upper limit of 610 events/day of pure ^{40}K β decays in the Borexino Fiducial Volume. On the other hand, use of the naive radial distribution for γ rays, or of the distribution simulated by Monte Carlo, implies a real measurable value ranging from 560 ± 250 to 670 ± 220 events/day in the Fiducial Volume.

It is worth noting that when the amplitudes of the supposed ^{214}Bi γ peak at 1.76 MeV in the four volumes are fit to Equation (9.6) using the three different models, the naive and Monte Carlo models yield a non-zero value for internal contamination with ^{214}Bi γ rays as well. (In both cases, the specific result is roughly 0.65 ± 0.30 events/day/ton. In the third

model, using the supposed ^{214}Bi peak amplitudes as a reference, the result is of course zero by assumption.) This is a bit odd because the maximum observed internal rate of $^{214}\text{BiPo}$ coincidences during the period of Runs 2300–2563 is never more than 2 events/day/ton. Very few internal ^{214}Bi decays should leak into the data sample in the 1.76 MeV peak, because coincidences were specifically excluded from the sample. The likely possibilities are as follows:

- The naive and Monte Carlo radial distribution functions do not model the actual radial distribution of the reconstructed positions of external γ rays very well.
- The amplitudes of the ^{214}Bi peaks are, just through an unfortunate chance, not in line with what would be expected statistically.
- The detection of coincidences in the CTF is much less efficient than generally supposed.
- The peak near 1.76 MeV is not actually the ^{214}Bi γ ray, but instead is from some other isotope.

Of these hypotheses, the first two above are most probable (the other two are mentioned for the sake of completeness). The first hypothesis implies that the ^{214}Bi radial fit should be taken most seriously. The second, however, leads to a directly opposite conclusion. The second hypothesis is supported by the observation that the number of ^{214}Bi 1.76-MeV events measured in the next-to-outermost radial shell (223 ± 86 events) is greater than the number measured in the outermost shell (215 ± 58 events), whereas the situation for the ^{40}K peak is the other way around (318 ± 48 events versus 428 ± 53 events); refer to Table 8.9. Unfortunately, if the second hypothesis is true, contamination of the Borexino scintillator by ^{40}K may potentially be a large problem. Further studies are recommended.